

Spacesuit Integrated Carbon Nanotube Dust Removal System: A Scaled Prototype

Dr.Kavya K.Manyapu*¹ and Dr.Pablo deLeon²
University of North Dakota, Grand Forks, ND 58202, USA

Dr.Leora Peltz³
The Boeing Company, Huntington Beach, California Province, CA 92647, USA Country

and

James R. Gaier⁴
NASA Glenn Research Center, Cleveland, OH 44135

Spacesuit dust mitigation has been a topic of high relevance and a critical path for future planetary exploration missions including Moon, Mars and Asteroids. A previous study demonstrated utilizing Carbon Nanotube (CNT) yarns as electrode wires embedded into coupons made of spacesuit outerlayer material. When a multiphase Alternating Current (AC) voltage signal was applied to this material, the spacesuit fabric repelled greater than 80% lunar dust simulant with particle sizes between 10-75µm in ambient conditions. As a continuation to this study, the feasibility of scaling this CNT embedded dust removal system on larger portions of spacesuit is currently under investigation. A scaled prototype representative of the knee portion of a planetary spacesuit utilizing specifics of the NDX-2 lunar spacesuit developed by University of North Dakota has been constructed. The outerlayer of this prototype is embedded with the CNT dust removal system and tested under various conditions. Fabrication of this system and results from the experiments are detailed in this paper.

Nomenclature

%DA	=	percentage of dust covering the fabric post cleaning operations
AC	=	clean area of the fabric evaluated
AdA	=	area of the fabric covered in dust post cleaning
%DB	=	percentage of dust covering the fabric prior to cleaning operations
AdB	=	area of the fabric covered in dust before cleaning
%DC	=	efficiency of the dust cleaning performance
AC	=	Alternating Current
CNT	=	Carbon Nanotube
EDS	=	Electrodynamic Dust Shield
EMU	=	Extravehicular Mobility Unit
EVA	=	Extra Vehicular Activity
ISS	=	International Space Station
MMOD	=	Micrometeoroids and Orbital Debris
SPIcDER	=	Spacesuit Integrated Carbon nanotube Dust Ejection/Removal
WFM	=	Work Function Matching coating
UND	=	Univeristy of North Dakota

¹ Visiting Researcher, University of North Dakota, Grand Forks, ND 58202, USA and *Flight Crew Operations Engineer, CST-100, The Boeing Company, Houston, 77058, USA.

² Professor, Department of Space Studies, University of North Dakota, Grand Forks, ND 58202, USA

³ Technical Fellow, Boeing Research and Technology, Huntington Beach, CA 92647, USA

⁴ Research Physicist, Space Environment and Experiments Branch, NASA Glenn Research Center, Cleveland, OH 44135, USA

I. Introduction

WHILE efforts are under way to revamp lunar exploration missions, return astronauts to the Moon and set-up habitats for long duration missions, the issue about lunar dust remains a concern. Lunar dust proved to be troublesome during the Apollo missions. The powdery dust got into everything, abrading spacesuit fabric, clogging seals and other critical equipment¹. Once inside the lunar module, Apollo astronauts were exposed to this dust when they removed their dust coated spacesuits. Lunar dust is electrostatically charged due to solar wind and exposure to UV irradiation. As such, NASA has identified dust as a major environmental challenge to overcome for future long duration missions to the moon.

This paper is a continuation to the research efforts previously conducted by the current authors on developing a spacesuit integrated dust cleaning system for lunar exploration missions². Leveraging NASA's concepts for dust mitigation on solar panels using the Electrodynamic Dust Shield (EDS), the Spacesuit Integrated Carbon nanotube Dust Ejection/Removal system (SPICDER) was conceptualized and tested. The SPICDER system proposed for spacesuit dust mitigation consists of parallel yarns made of Carbon Nanotube (CNT) flexible fibers embedded into the outerlayer of the spacesuit that act as electrodes wires. These CNT fibers when activated utilizing a multi-phase Alternating Current (AC) voltage signal, would levitate and push the dust off the surface of the material. The system can be further augmented with Work Function Matching (WFM) coating made of lunar dust (in this case lunar simulant) that works to lower the adhesion of dust to the surface, thereby preventing further accumulation of dust. The combination of the CNT electrode network along with the WFM coating is proposed to provide an enhanced dust cleaning strategy for use in spacesuits for lunar missions.

Previously, the research team demonstrated the feasibility of using SPICDER for dust mitigation of flexible surfaces via experiments on coupons made of spacesuit orthofabric material embedded with CNT fiber electrodes. Experiments demonstrated that the SPICDER system is capable of repelling > 80% of JSC-1A lunar dust simulant particles with grain sizes between 10-75 μm in ambient conditions, in both dynamic and static dust loading². This cleaning using the SPICDER system resulted in less than 10% of the fabric area covered in residual lunar dust. In the current paper, the development and testing of a scaled functional prototype, representative of the joint knee section of a planetary spacesuit embedded with the SPICDER system are discussed. Results are analyzed to assess the validity of the scalable functionality of the SPICDER system. The prototype constructed for this research to demonstrate SPICDER's scalability utilizes specifics of the NDX-2 lunar spacesuit developed by University of North Dakota (UND). It is expected that the scaled SPICDER system provides comparable results observed during coupon testing. The paper subsequently provides recommendations for manufacturing when scaling the system to cover larger areas of the spacesuit based on lessons learned from building and testing the prototype.

II. Methods and Materials

A. Test Objectives

The primary objectives of the experiments conducted on the scaled prototype are two-fold:

- Assess the feasibility of manufacturing the SPICDER system to a full-scale spacesuit leg, specifically the knee-joint section. The knee portion has been chosen because of the substantial evidence from Apollo missions on the dust coverage and abrasion of the knee area of the suit and the complexity for manufacturing a joint section.
- Validate the dust cleaning performance of the SPICDER system on a scaled model that was observed on small scale demonstrations. The main performance metric in the scaled SPICDER system is the residual (%) coverage of dust remaining after cleaning operations. Successful mitigation is defined as residual dust coverage less than 25% of the spacesuit fabric area shielded by electrodes. This performance metric is driven by the requirement that the thermal effects of the residual dust on the spacesuit are allowed to degrade at most 20% of the localized area of the suit's radiative thermal capability³.

Secondary objectives encompass validating functionality of SPICDER on a pressurized suit, identifying performance differences if any for straight and bent (flexed) knee conditions, and identifying limitations of SPICDER performance. Experiments were conducted in ambient conditions. Vacuum testing was conducted using coupons due to size constraints of the vacuum chamber available. Results of the vacuum test will be part of a future publication.

B. Prototype Development

The scaled prototype is a knee-joint section of a spacesuit. Dimensions for the model are based on the NDX-2 lunar spacesuit prototype developed by UND under a NASA grant to demonstrate usability for extended lunar missions with operating pressures of 4 psi⁴. NDX-2 features a malleable hard upper torso with a rear entry closure and soft lower torso elements. The restraint layer knee joints are an asymmetrical semi-toroid joint with elements from flat pattern joint. Figure 1 shows the NDX-2 lunar Extra vehicular Activity (EVA) spacesuit prototype without the thermal

insulation and outerlayer cover. The pressure bladder-restraint assembly is covered by orthofabric or similar candidate fabric to protect the internal components of the suit from dust, abrasion, flame resistance, Micrometeoroids and Orbital Debris (MMOD), and for thermal insulation.

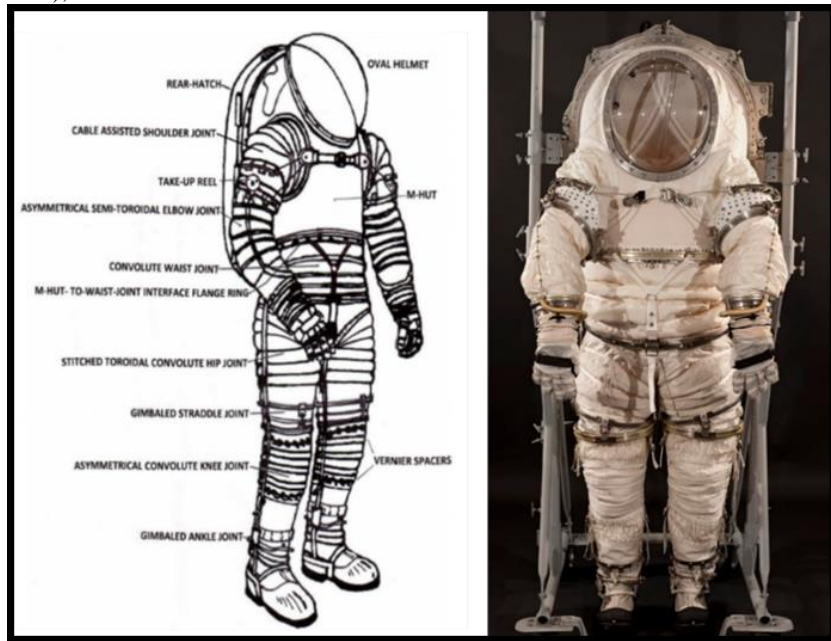


Figure 1. **NDX-2 Lunar EVA spacesuit prototype built at UND⁴**. Model shown here is only the pressure garment with the white restraint layer. Orthofabric or other candidate fabric would cover the outerlayer

C. Construction

There are two aspects of the prototype construction. First is the fabrication of the outerlayer made of orthofabric material and the placement of the CNT fiber electrodes. Second is the pressure bladder with the restraint layer, constructed separately with aluminum sealed ends to facilitate build of a module that can be pressurized to conduct experiments on a pressurized module representative of the operational state of a spacesuit during a lunar surface EVA.

1. Outerlayer Construction and SPICDER Fabrication

The outerlayer for the prototype was designed based on a flat pattern joint design utilized in the International Space Station (ISS) Extravehicular Mobility Unit (EMU) outerlayer and the NDX-2 lunar spacesuit outerlayer.

• Flat-Pattern Joint Outerlayer

The flat-pattern design is a commonly used pattern in spacesuit joint design, especially the outerlayer where joints are all fabric in most spacesuits. The flat pattern joint is an all fabric joint fabricated using gore segments that are shaped as pleats with excess material built into the fabric on the outer sides of the joint. These gores are tucked into a series of transverse pleats/patterns in telescopic fashion. When pressurized and flexed, these pleats balloon out and form a series of semi-convolute shapes⁵. The excess material built into the tensile side (front of the knee) of the joint provides

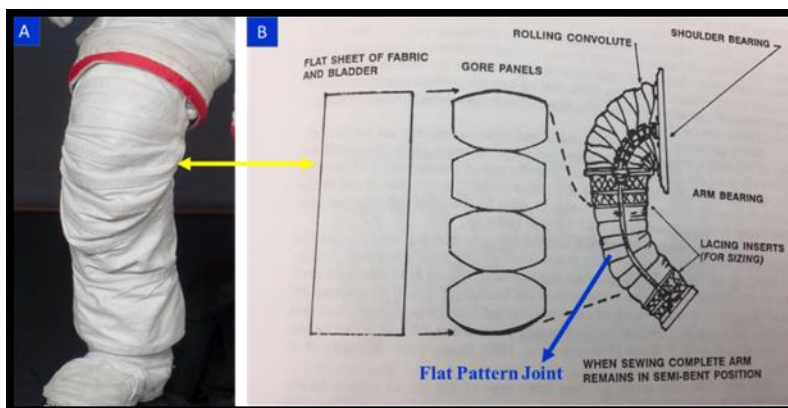


Figure 2. [A] Flat pattern knee joint of ISS EMU (unpressurized), [B] Flat Pattern knee joint concept⁵

sufficient material to stretch when the knee bends or flexes allowing the internal volume of the space suit to remain approximately constant. On the compressive side (back of the knee), the gores roll over one another when the joint bends. Longitudinal restraining straps are stitched along both sides of the joint (along the neutral axis). Shown in Figure 2 is an example of flat pattern joint from Ref 5., and a close-up of the unpressurized ISS EMU outerlayer flat-

pattern joint. The fabric flat pattern joint designed for the current experiments utilizes gores as shown in Figure 2. After the outerlayer was fabricated, it was embedded with the CNT electrode network in the orientation shown in Figure 3.

• CNT fiber Placement and Orientation

The electrode characteristics for the scaled model were based on parameters that provided optimal results during the proof of concept demonstrations using small scale coupons², simulation studies³, and orientation of the weave of the orthofabric material, that provided optimal dust cleaning performance using the SPICDER system.

CNT fibers on the model were embedded such that the parallel electrodes were circumferentially oriented throughout the length of the electrode covering the front section of the knee. The major factor impacting the orientation of the fibers was ease of manufacturing and terminating electrodes circumferentially rather than longitudinally. Another factor impacting electrode orientation is that the pleats expand longitudinally. Embedding the electrodes longitudinally may therefore constrain opening of the pleats when the knee flexes. However, this was only an assumption and was not physically confirmed. A third factor impacting electrode orientation was the direction of the electric field wave which in this case travels from top of the leg to the bottom of the leg moving the particles in the longitudinal direction. The assumption is that the particles would be moved towards the bottom of the leg with gravity assisting the ‘fall’ of the particles. Forward work to validate this assumption could be to perform SPICDER tests with simulant in a microgravity environment to understand the behavior of dust in partial gravity. This is currently outside the scope of the current paper.

The CNT fibers were embedded using the same techniques utilized for the coupons where each CNT fiber is carefully driven in the warp direction under every weft thread using a sewing needle. Automated methods for fabric making with the CNT fibers were not feasible currently due to the unavailability of machinery and due to the novelty of the method, specifically in terminating the ends of the electrodes. Each of the individual CNT fibers was terminated inches ~3 inches beyond the restraining strap to make necessary electrical connections. CNT fibers of the respective phase are grouped together and attached to a conductive termination adapter (Copper Tape) placed longitudinally and stitched into the outerlayer. Kapton tape and adhesive glass fiber cloth were utilized as insulative termination adaptors to isolate electrode groups of distinct phases. Figure 4 illustrates the final outerlayer embedded with the CNT fiber electrode network at pre-specified spacing, diameter and number of phases.

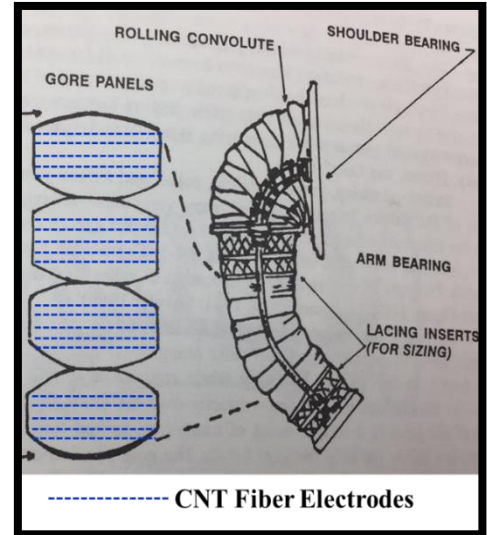


Figure 3. Orientation of CNT Fiber electrodes

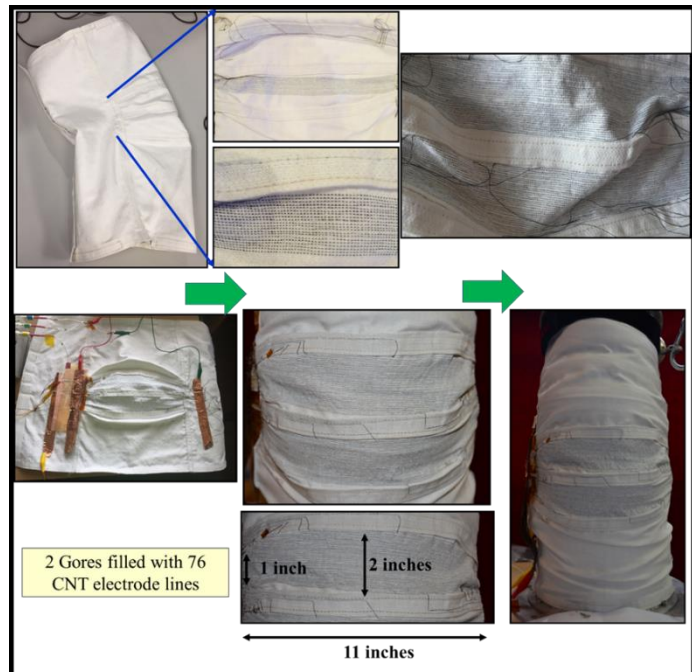


Figure 4. Joint-knee section embedded with CNT electrodes. Two gores filled with 76 number of electrodes with electrode characteristics show in Table 1.

2. Pressure Bladder-Restraint Assembly Construction

The pressure bladder along with the restraint layer for the knee section are constructed as one unit, separately from the outerlayer. Either ends of the leg-knee section are sealed with aluminum plates. The top and bottom of the module have provisions for pressurizing the module. The bottom valve interface is used to pressurize the module which is outfitted with a pressure gauge. The outerlayer with the embedded CNTs is attached to the pressure-restraint assembly using Velcro around the circumference of the top and bottom of the outerlayer. The pressure bladder utilized for the construction is the polyurethane coated nylon membrane, which is the same as the NDX-2 and the ISS EMU pressure bladders. The restraint layer is a nylon rip-stop which has similar characteristics as the ISS EMU restraint layer. Figures 5 through 7 show the pressure bladder-restraint assembly section of the prototype and the complete assembly with the outerlayer. The thermal insulation material (Aluminized Mylar) was not built into the outerlayer prototype due to constraints in fabrication and since no data below the outerlayer was being collected. It is anticipated that because the insulation thermal layers are built into the outerlayer itself with a thickness less than 0.7 mm (per ISS EMU), there would not be an effect on the outer surface dust cleaning performance and the maneuverability of the prototype to different knee angles. The operational pressure of the module was kept at/below 3 psi to prevent accidental burst of the module for the duration of the experiments. Since the module would undergo >50 pressurization cycles, it was decided to not go beyond this pressure although historically flight operating pressures for U.S spacesuits have been between 3.5-4.3 psi. All test runs were conducted between 2.5-3 psi. It is anticipated that the geometry of the pressurized unit at 4.3 psi compared to 2.5 psi are not substantially different. The module is very rigid once pressurized to 2.5 psi. The results from the tests are applicable to a fully pressurized unit with no expected differences in the dust cleaning performance. Table 1 provides the details of the complete system configuration with materials, geometry and CNT properties utilized.

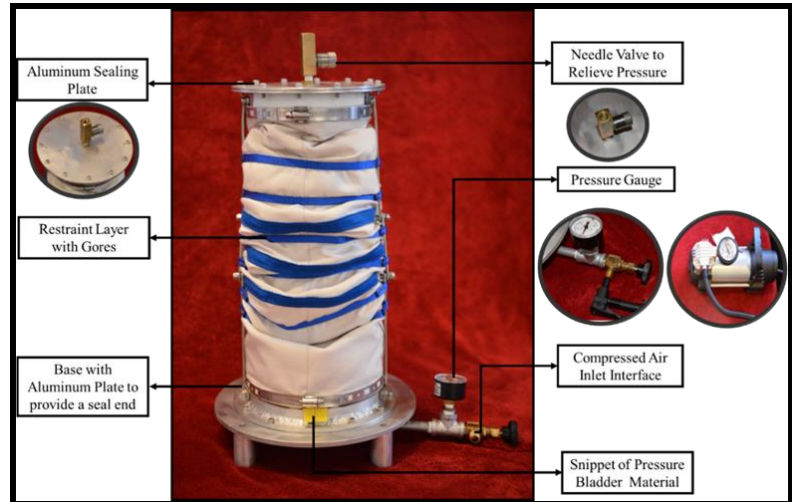


Figure 5. Pressure bladder-restraint assembly prototype

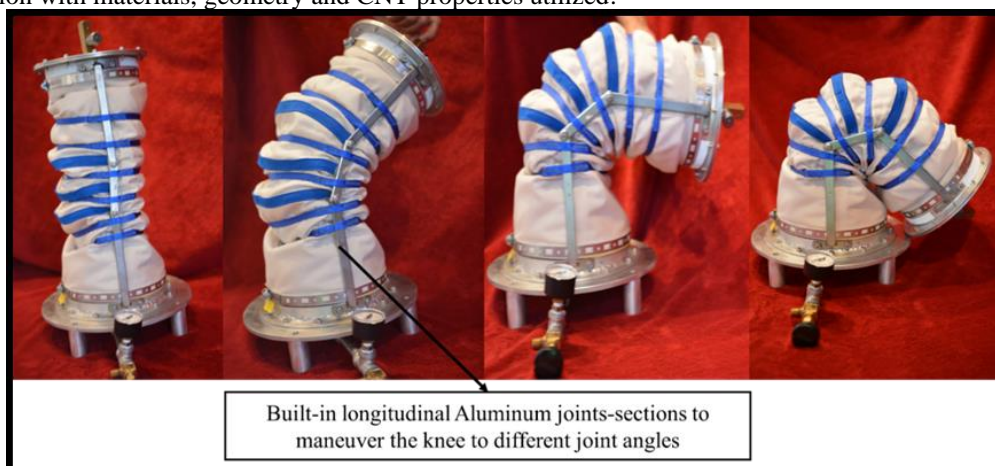


Figure 6. Maneuverability of the prototype when unpressurized

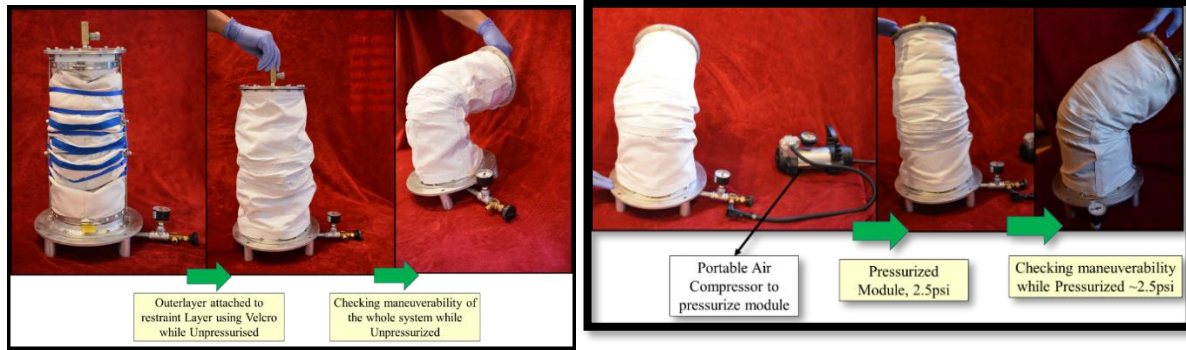


Figure 7. [Top] Attaching the outerlayer over the pressure-restraint system when module is unpressurized, [Bottom] Maneuvering the knee to various angles after pressuring. Note that the knee could not be flexed beyond 45°

Table 1. Configuration of the Scaled Prototype

Materials	
Suit Materials	
• Outerlayer	Orthofabric
• Pressure Bladder	Polyurethane coated Nylon (same as EMU)
• Restraint Layer	Nylon Rip-stop (same characteristics as EMU)
Electrode Material	CNT fibers uninsulated
Seals	Aluminum plates
Termination Adapters	
• Conductive	Copper Tape
• Insulative	Kapton, Glass Fiber Tape

Geometry	
Length of entire unit	22 inches
Length of outerlayer	16 inches
Diameter (top)	20 inches
Diameter (bottom)	24 inches
Number of gores	2
Number of electrodes/gore	38
Neutral angle (pressurized)	15°

CNT Electrode Properties	
Ply / Stranding	7/32 AWG
Diameter	212±7 µm
Length of electrode per line	10 in
Electrode Spacing	1-1.2 mm
Linear Density	25.7±0.4 tex
Density	0.72 g/cm ³
Resistance	18.4±0.2 Ω/m
Electrical Conductivity	1.5±0.1 MS/m
Specific Conductivity	2100 Sm ² /kg
Tensile Strength	835±40 MPa
Strength (Tenacity)	1.1 ±0.1N/tex

Environmental Parameters	
Temperature	22-25°C
Ambient Pressure	14.7 psi
Relative Humidity	39-41%
Lunar Dust Simulant	JSC-1A 50-75µm JSC- 1A 10-50 µm
Suit Pressure	2-2.5psi

Operational Parameters	
Input Voltages	880-970 V
Frequency	5 Hz
Waveform	Square
No. of Phases	3
Dust Loading	Amount of dust
• Dynamic	1g
• Static	1g

III. Experimental Set-up

The entire module (knee-joint with the outerlayer layer, restraint-pressure bladder assembly) was placed on a bench top using a stand to hold the module at the specified angle. A plastic bottle with pierced lid was utilized to drop the dust over the knee section. 3-phase tunable power electronics from NASA that was previously utilized for the coupon experiments was utilized for this experiment. Each of the conductive termination adapters for the 3 phases on the outerlayer was connected to the power supply using three insulated wires. The knee was pressurized using a portable Husky 120-Volt air compressor that interfaces with the valve on the bottom of the module. Figure 8 shows the complete module and test set-up.

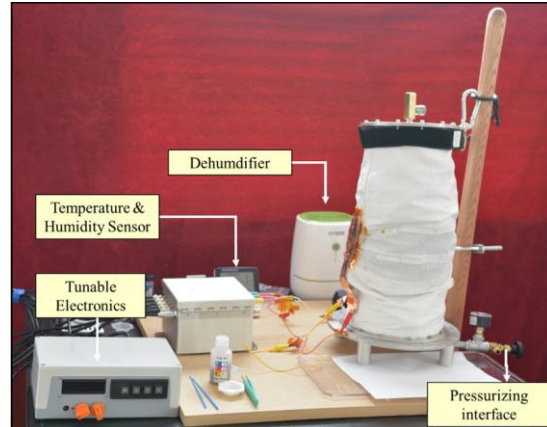


Figure 8. Experimental set-up of the scaled prototype

A. Test Conditions

The SPICDER system on the scaled knee-joint section was evaluated at three bend (flex) angles of the knee under two specific dust depositing conditions similar to the ones implemented on the coupon tests. 1) Dynamic Drop test and 2) Static test. Three runs per angle were performed for each dust loading condition (dynamic and static) to identify repeatable performance, and data was collected and analyzed on two consecutive runs. JSC-1A lunar dust simulant with grain sizes 50-75 μm and 10-50 μm was utilized. All tests were conducted at room temperatures in the range 23-25 $^{\circ}\text{C}$ and RH in the range 39-41%.

1. Dust Loading Conditions

In the case of 'Dynamic Drop test', the CNT fibers were first energized prior to depositing dust simulant over the knee. While the system was active, 1g of lunar dust simulant was continuously deposited/dropped over the entire knee area with electrodes. This test case is presumed to represent lunar dust actively interacting with the suit when an astronaut is walking on the surface of the moon during an EVA and dust is being kicked up. In the static test case, a measured amount of simulant was deposited over the knee covered with CNTs prior to activating the system. This condition represents a scenario where the suit is pre-disposed to dust which has statically adhered and coated the suit during an EVA.

The prototype was positioned perpendicular to the ground as shown in Figure 8, in an orientation representative of an astronaut standing/walking in a suit. Dust was dropped at an angle to the knee as shown in Figure 9. For the dynamic test, the dust was continuously dropped over the knee sweeping left to right to cover the area. For the static test, the dust was dropped to cover the knee area prior to activating the system. The knee at a 15° angle was nearly vertical when placed perpendicular and was a challenge to keep the dust in position due to gravity. For this angle, the prototype was also tested in the horizontal position so that sufficient dust stayed on the knee prior to activating SPICDER for the static test. Using both orientations provided sufficient evidence that the SPICDER system was clearing the dust. For the coupon tests, dust was dropped perpendicular to the coupon for both the dynamic and



Figure 9. Dust loading method

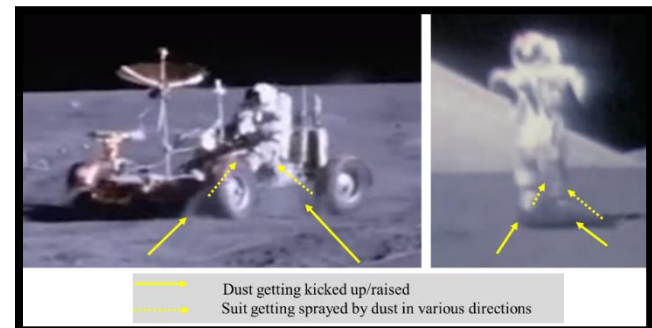


Figure 10. Examples of directions through which spacesuit is exposed to dust during surface operations (Background image credit: NASA)

static tests. On the lunar surface, astronauts will be exposed to dust in various directions- while walking the dust will get kicked up, during drilling operations dust would spread out and 'fall' on the suit, while on the rover, the dust gets picked up by the wheels and sprayed onto the suits as seen in Apollo missions (See Figure 10). Therefore, the dust exposure during the experiments conducted here utilize a subset of these different modes to provide an approximation of the dust exposure to validate the scalable functionality of the SPICDER system. Future work would involve implementing test setups of the scaled SPICDER system in realistic dust exposure settings simulating surface operations. For example: one test method would be to set-up an experiment in the lunar regolith bin at NASA KSC or the wind tunnel similar to the ones performed on the NDX-1 spacesuit study by Ref 6.

2. Bend Angles

The bend angles correspond to the range of motion of the knee when the astronaut is walking in the suit. Dust loading and cleaning for three specific angles of the knee are evaluated: 1. One that corresponds to the neutral position of the knee when the suit is pressurized (no flex). The neutral angle of the knee was determined after the module was pressurized prior to beginning the test procedures. This was observed to be approximately 15° during the experiments. 2. An intermediate angle of 30°. 3. A third angle of 45°.

The original plan was to flex the knee to 90° for a fourth configuration. However, the knee could not be flexed to 90° when the module was pressurized due to rigidity. Once pressurized, it was difficult to bend the knee module

beyond 45-50° and hold it place. To prevent any damage to the test article, tests were limited to the 45° angle. Figure 11 and Table 2 provide a representation of the three angles tested with the two dust loading conditions and test cases performed. It is anticipated that for normal walking motions of the astronauts most of the movements are in the range of 10°-60°, except when they sit on the rover or when they kneel. The results of the experiments conducted here can be extrapolated to 60°-90° without significant differences in cleaning performance.

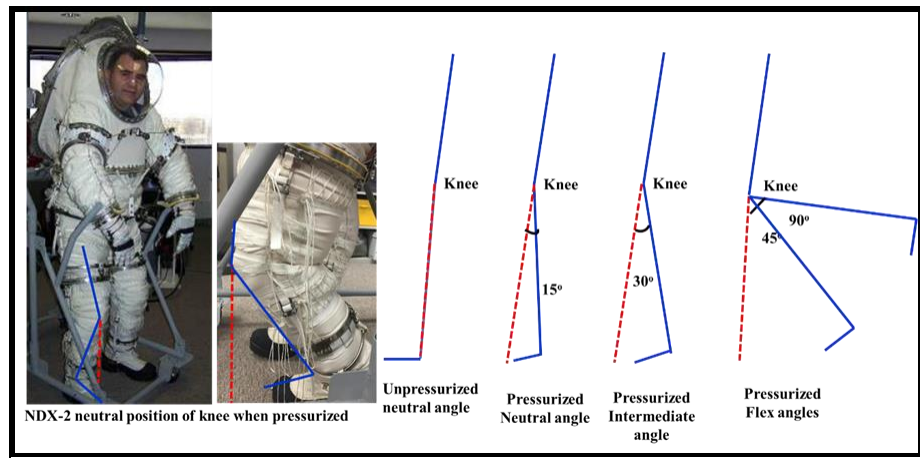


Figure 11. Angles of knee tested for dust cleaning performance of SPICDER. 90° was planned but could not be tested when pressurized due to module constraints

Table 2. Test Conditions tested to investigate scalable functionality of the SPICDER system

#	Dust Loading	Simulant (μm)	Knee Bend Angle (degrees)	Module Pressure (psi)	Temperature (°C)	Relative Humidity %	Voltage (V)	Frequency (Hz)
1	Threshold Calibration		Neutral- 15°	2.5	24	40	1010	5
2	Threshold Calibration		30°	2.5	24.1	40	1050	5
3	Threshold Calibration		45°	2.5	24	40	1090	5
4	Dynamic	50-75	Neutral- 15°	2.5	24	40	945	5
5	Dynamic	50-75	30°	2.5	23.2	40	945	5
6	Dynamic	50-75	45°	2.5	23.8	39	970	5
7	Dynamic	10-50	Neutral- 15°	2.5	23.5	40	900	5
8	Dynamic	10-50	30°	2.5	22.9	40	945	5
9	Dynamic	10-50	45°	2.5	24.1	39	970	5
10	Static	50-75	Neutral- 15°	2.5	23.9	40	900	5
11	Static	50-75	30°	2.5	24.9	40	945	5
12	Static	50-75	45°	2.5	24.1	40	970	5
13	Static	10-50	Neutral- 15°	2.5	24.5	40	900	5
14	Static	10-50	30°	2.5	24.4	40	945	5
15	Static	10-50	45°	2.5	23.7	39	970	5

B. Test Procedure

- a. Breakdown Voltage Calibration (runs 1-3 in Table 2): Prior to conducting the dynamic and static tests, voltages where breakdown starts to initiate for each bend angle were calibrated. This was achieved by first energizing the electrodes without dust loading and slowly increasing the input voltage starting from 100V in 50V increments until arcing is evident. The voltage at which arcing occurs (breakdown) was noted for each bend angle.
- b. Test Runs (Dynamic and Static, runs 4-15 in Table 2): When data was gathered in step a, the actual experiments with dust loading using the dynamic and static setting were conducted beginning with voltage values 200V below the breakdown voltage. The operating voltages where best performance occurs for each bend angle were identified and utilized for the experiments (~100-50 V below the breakdown voltage).

C. Data Collection and Analysis Methods

Data was primarily collected using 1. Visual Observations, 2. Microscopic and Macroscopic imaging and 3. Videography. For the dynamic drop tests, continuous video was recorded while dust was dropped. The knee area was imaged in place after the system was powered off using a Celestron® handheld digital microscope and a Canon® digital SLR camera. For the static test, the knee area was imaged prior to dust deposition and after cleaning operations when the system was powered off. Microscopic images using the digital microscope were taken at 20X magnification to record the state of the fabric and dust distribution. Video during static cleaning operations was also recorded. Both the dynamic and static tests were repeated multiple times for each bend angle to observe consistency of dust cleaning.

Qualitative and quantitative analysis were used to assess the performance of the SPICDER system and its scalable functionality with data obtained from two consecutive runs. The dust cleaning capability was evaluated using 1) Visual inspection via the videography data and images collected during the experiments to document observable dust cleaning capability for the qualitative aspect of the analysis 2) For the quantitative aspect, images were analyzed using ImageJ® software to estimate the overall percentage of dust covering the orthofabric before and after cleaning. Due to the large area of the knee and imaging capability using a digital microscope, for each run, analysis was performed on five smaller sections of the knee, each with an average area of 6mm x 6mm on five separate locations on the knee. The locations were chosen based on worst case dust coverage post cleaning operations. Figure 12 shows ImageJ color thresholding and particle counting used to process the images.

- Voltage values

Two voltage values for each bend angle are reported. The threshold voltages where breakdown occurs, and the operating voltages of the system used for dust cleaning operations where best performance was observed. Threshold voltages are collected for each bend angle are compared to the threshold voltages observed during coupon tests where breakdown initiated. Results from the experiments and simulation for these breakdown voltages are compared and differences analyzed.

- Evaluating Dust Cleaning Performance

The percentage of dust coverage on the fabric area after cleaning operations has been utilized as the key parameter to evaluate dust cleaning performance. Figure 13 illustrates the steps and equations utilized to analyze the cleaning performance of the system for the dynamic and static dust loading conditions. The results from the three equations represented in the flow chart are reported in the subsequent results and discussion sections. The parameters of these equations are described below.

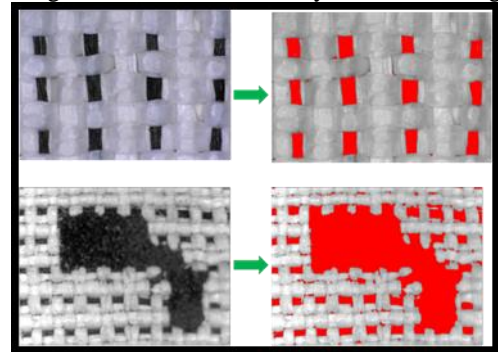


Figure 12. Image processing using ImageJ® software to estimate dust coverage area. Shown here are examples of a clean fabric estimating CNT area and a sample covered in dust before cleaning operations.

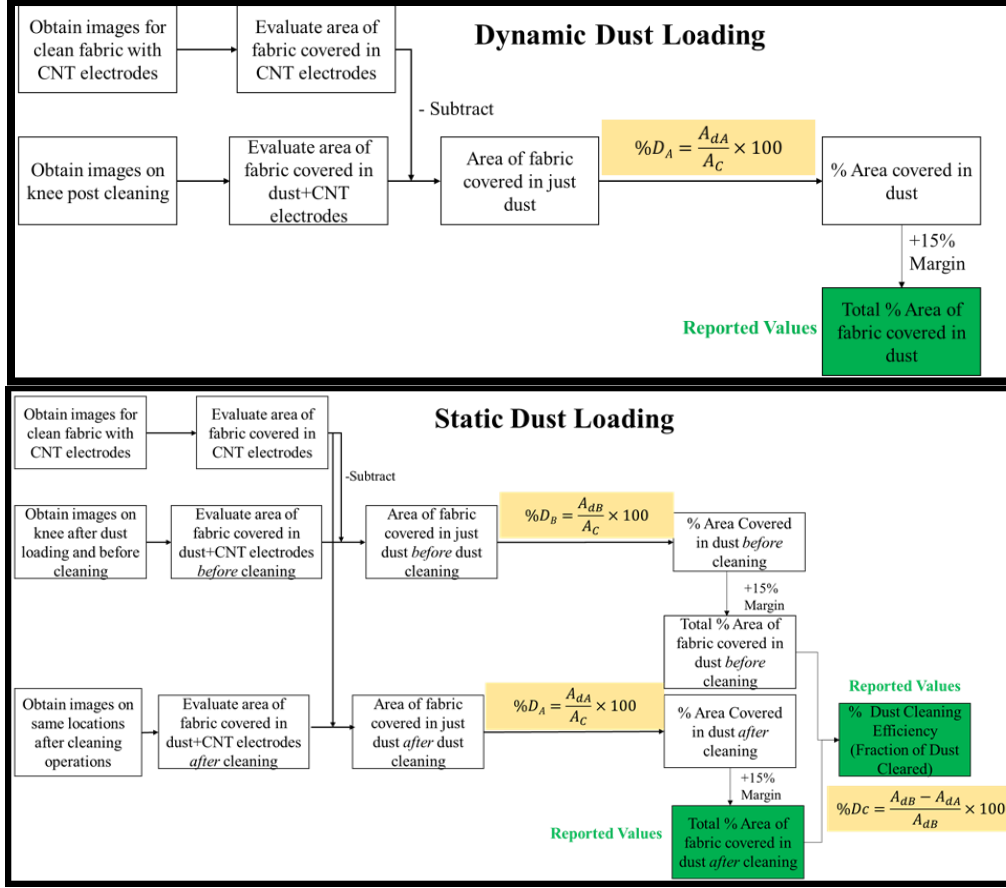


Figure 13. Flow chart illustrating the method to analyze percentage of fabric area covered in dust before and after dust cleaning and evaluation of SPIcDER's dust cleaning performance

- **Dynamic Dust Loading:** The percentage of dust covering the fabric is calculated using Equation 1, where $\%D_A$ is the percentage of dust covering the fabric post cleaning operations, A_C is the clean area of the fabric evaluated, A_{dA} is the area of the fabric covered in dust post cleaning. This value is obtained by subtracting visible CNT area to obtain area covered in just dust post cleaning operations.

$$\%D_A = \frac{A_{dA}}{A_C} \times 100 \quad (1)$$

- **Static Dust Loading:** The percentage of dust covering the fabric before dust cleaning is calculated using Equation 2, where $\%D_B$ is the percentage of dust covering the fabric prior to cleaning operations, A_C is the clean area of the fabric evaluated, A_{dB} is the area of the fabric covered in dust before cleaning.

$$\%D_B = \frac{A_{dB}}{A_C} \times 100 \quad (2)$$

The percentage of dust covering the fabric after dust cleaning for static test is also calculated using Equation 1. The efficiency of the dust cleaning performance ($\%D_C$) of the SPIcDER system is then calculated using Equation 3 which provides the percentage of dust removed from the fabric due to cleaning compared to the original dust on the fabric before cleaning operations. This equation is applicable specifically for the static tests. For the dynamic tests, visual operations will be used to estimate the efficiency based on the equation 1. A 15% margin has been added to all the performance values for a conservative approach. Results obtained are compared with the coupon tests, illustrated as 0° on the figures in subsequent sections.

(3)

$$\%D_C = \frac{A_{dB} - A_{dA}}{A_{dB}} \times 100$$

IV. Scaled Model Test Results and Discussion

A. Threshold/Breakdown and Operating Voltages

The voltage where the surrounding medium breakdowns due to electric discharge is dependent on the electrode configuration and the surrounding gas pressure. It was observed that knee angle impacts the fabric layout, i.e., the fabric might have wrinkles/folds/creases when unpressurized and when the knee is in a neutral position (no flex angle) when pressurized. These creases in the fabric may stretch/smooth out when the knee is in a flexed position. Therefore, the angles of the knee have an influence on how the embedded electrodes interact (spacing and overlap). There might be areas where the fabric creases so much that the electrodes potentially overlap impacting the value of breakdown voltage. When pressurized, the pressure inside the module helps the outerlayer fabric to bubble outward allowing smoothing out of the creases. When flexed, these creases smooth out further. Figure 14 illustrates the fabric layout for unpressurized and pressurized module. Calibration of the threshold voltages for the three knee angles was conducted with the module pressurized at 3 psi. Table 3 lists the observed voltages at the three angles tested and Figure 15 illustrates the difference in the threshold voltages observed during the knee experiments with results from simulation and coupon experiments for electrode spacing of ~1.2 mm.

Table 3 Breakdown and operating voltages during experiments at knee angles tested

Knee Angle	V _B from Experiments	V _B from Simulation ³	Operating Voltage	Frequency
15°	1010 V	1350	900-945 V	5 Hz
30°	1050 V	1390	945 V	5 Hz
45°	1090 V	1430	970 V	5 Hz

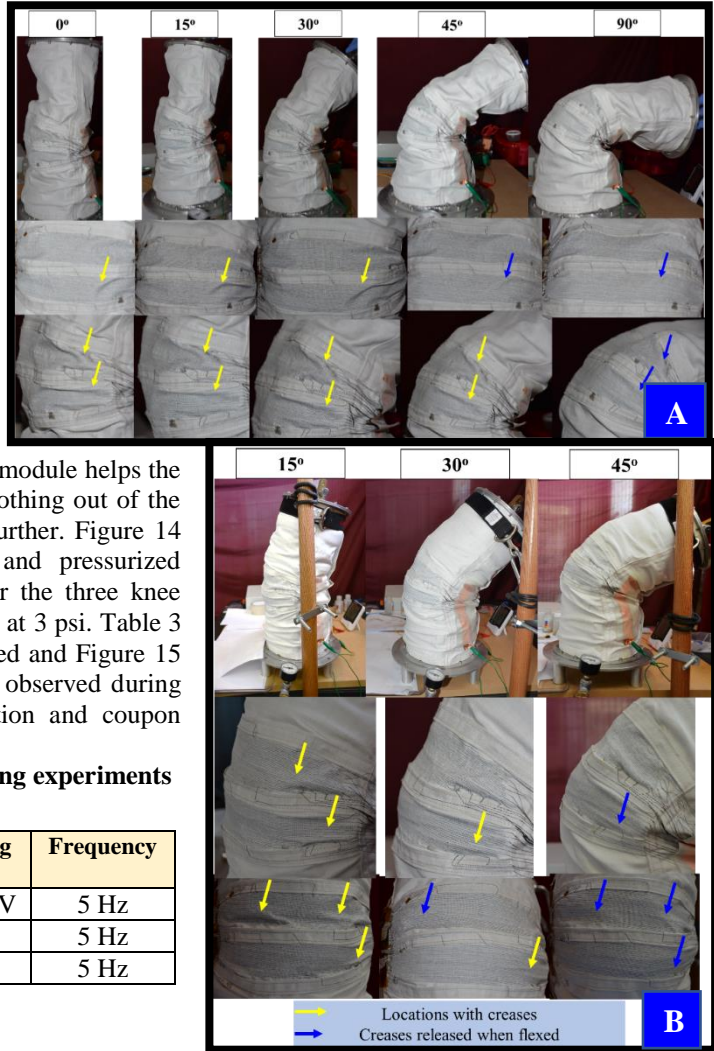


Figure 14. [A] Unpressurized and [B] Pressurized module. Arrows point to creases in the knee area. Yellow arrow represents creases in the fabric, blue arrow shows areas where creases have smoothed out once pressurized

V. Discussion

A. Threshold Voltages

1. Difference in Threshold voltages between the knee angles:

Both experimental and the simulation data show that there is a gradual increase in the voltage where breakdown initiates as the knee bend angle increases. The increasing trend of the threshold (breakdown) voltages for the 3 angles observed in the experiments correlate well with the trend observed in simulations (Figure 15 A). There are two reasons predicted for the increase in the breakdown voltage as the knee angle increases: First, when the fabric is pressurized at lower angles, due to the nature of the fabric and patterning of the joint section, creases/folds develop in the fabric. As the knee flexes to a higher angle, these creases on the knee start to unfold, smoothing out the fabric. Consequently, at the lower angle, the electrodes within the creases may start to overlap and compromise the electrode spacing (lower than 1.2 mm in this case) increasing the risk of breakdown occurring at lower voltages. As the knee angle increases and creases smooth out, the electrode spacing is now at the intended spacing, and the voltage at which breakdown occurs is higher than at lower angles, as dictated by the Paschen law. While the trend for breakdown voltage within both the experimental and simulation data show similar increase in the breakdown voltage with an increase in the knee flexion (~40 V increase with every 15° increase), the impact due to creases/folds are not replicated in the simulation. The difference between the experimental and simulation data however for each angle (~340 V reduction in breakdown voltage noticed between experiments compared to simulations for each angle) could be associated with these unanticipated folds of the fabric where breakdown initiated. Additionally, experiments demonstrated that the risk for breakdown is not at the corner of the knee, there is no significant difference in how the fabric bunches at the corners of the knee in both 15° and 45°.

Second, as the knee flexes and the fabric bends, there is a slight stretch in the fabric, the consequence of which is an increase in the electrode spacing. With an increase in electrode spacing, there is a corresponding increase in the breakdown voltage as dictated by the Paschen curve. Data from the simulations show that there is a minor increase in the electrode spacing ranging between 0.1 μm upto 140 μm depending on the location of the electrodes along the curvature due to the intrinsic property of the curved geometry surface (See Figure 16). Although the simulations do not replicate the fabric properties of the orthofabric material utilized in the experiments, electric field simulations for the four angles, show that voltages where breakdown initiates increase as one flexes the knee from 15° to 90° degrees at the rate of ~ 40 V increase for every 15° increase in the knee flexion (See Figure 15). Due to this inherent increase in the electrode spacing due to geometry shown in the simulations combined with the experimental data, it could be concluded that the electrode spacing differences between the angles causes the observed increase in breakdown voltage. To mitigate issues with breakdown during testing, the SPICDER system was operated ~ 100 V below the threshold voltage at each angle which corresponds to operating voltage ranges between 900-970 V for the three knee

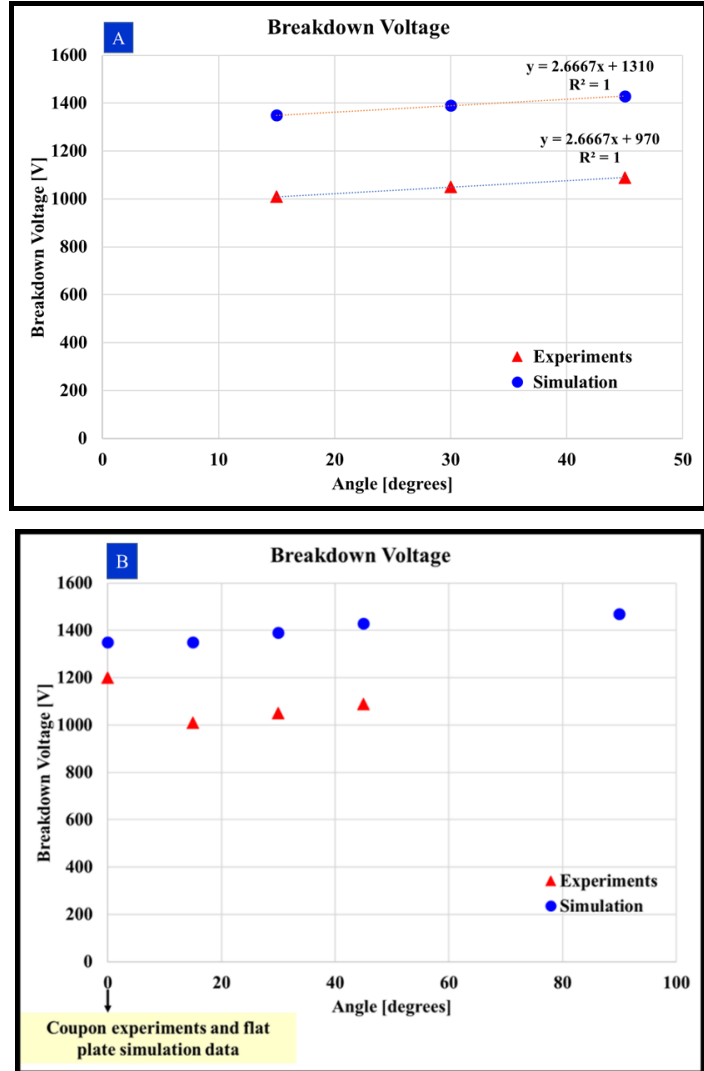


Figure 15 [A] Correlation of experimentally observed breakdown voltages with simulation produced breakdown voltages for the three angles tested. [B] Breakdown voltages for 90° and coupon experiment data. Here 0° represents the results from the coupon tests²

angles. The performance of the system with these operating voltages was comparable to the results obtained on coupon tests.

2. Difference in threshold voltage between the coupon and scaled prototype experiments

The threshold and operating voltages during the knee prototype tests were ~100-150 V lower than the coupon experiments (1010-1090 V on knee versus 1150-1200 V on coupons). Figure 15B illustrates this difference in threshold voltages. While the threshold voltages for the knee experiments was anticipated to be similar to that of the coupon tests due to the same average electrode spacing (~1.2 mm), three potential factors have been identified contributing to the decrease in the voltage, (1) Fold/creases (explained in previous section) (2) Inconsistent electrode spacing due to manufacturing process (3) fraying/hairs sticking out from the uninsulated CNT electrodes. As explained previously, due to the nature of the fabric layout (pleats) within the knee section, we expect to see creases in the fabric, specially at lower angles. There were areas where the electrode spacing of the consecutive CNT electrodes was compromised due to folds/overlap causing breakdown at lower voltages than anticipated. In addition to the contribution from irregular spacing within the electrodes as part of the manufacturing process (next paragraph), minor creases in the fabric even at the flexed position were discovered to be one of the reasons for lower threshold voltages on the scaled prototype when compared to the coupon experiments.

Second, the coupons previously fabricated were much smaller samples relative to the scaled prototype. The ability to manually embed CNT electrodes and adjust the spacing and alignment of the electrodes was relatively easy on smaller coupons. However, with the larger prototype, embedding CNT electrodes manually was labor intensive and although care was taken to align the electrodes within the warp threads, there were sections where it was difficult to pull the CNT electrodes under the weft threads. Once the entire electrode line was embedded, it was not easy to adjust the spacing between two consecutive electrodes over large areas. Consequently, certain sections of the knee had electrode spacing less than other areas and vice versa (Figure 17).

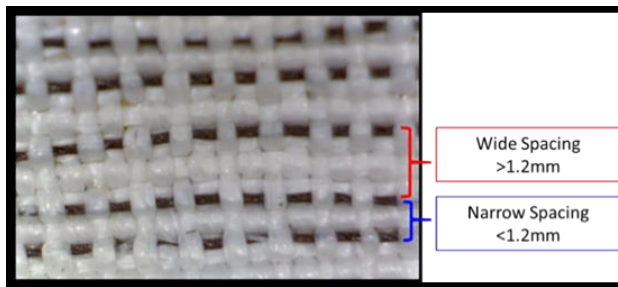


Figure 17. CNT electrode spacing irregularities using manual methods on scaled prototype

diameter electrode ‘thread’ required for dust cleaning. As such the electrodes may have localized sections where micron sized CNT fibers might be sticking out of the electrode pattern as a result of handling electrodes during the manual weaving process. On the coupons, care was taken post fabrication to verify that the CNT electrodes were aligned, and any fiber misalignment was rearranged accordingly. For the larger prototype, it was physically not possible to go through nearly 100 electrodes along the length of each electrode to check for the fibers and adjust. Therefore, it is anticipated that lower voltages were a result of reduced electrode spacing in a localized area due to frayed fibers. This issue can be certainly overcome by insulating the CNT electrodes in a flexible insulation material that would prevent fraying of the electrode fibers.

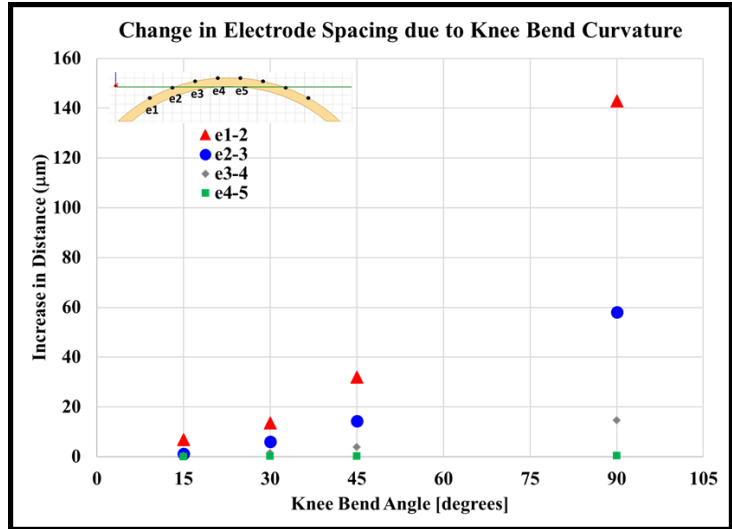


Figure 16. Increase in electrode spacing between each electrode group based on knee angle

While increase in the electrode spacing increases the voltage at which breakdown occurs, due to areas with <1.2 mm electrode spacing, breakdown initiated at lower than 1150 -1200 V as observed during the coupon tests. Hence, the threshold voltages of the knee were lower for all 3 knee angles when compared to the coupon tests (0°). These inconsistencies occurred due to the fabrication process and can be prevented by using automated weaving methods. Recommendations to overcome such electrode spacing inconsistencies are described in the next section

Third, the electrodes embedded into the knee are uninsulated wires. These CNT electrodes are made of several CNT fibers aligned together forming the larger

B. Key Observations during Dynamic and Static runs

Dust was visibly cleared during both the dynamic and static test cleaning operations over the areas where CNTs were embedded, particularly the 50-75 μm in all knee angle positions. Figures 18-20 illustrate the cleaning ability of the SPICDER system during both test conditions. Operating voltages had to be increased with increase in flex angle to obtain same performance. This correlates well with simulations conducted (not detailed in this paper) for curved surface due to increased electrode spacing. Dust was also dropped on areas where there were creases and folds where CNTs were embedded and dust visibly cleared even from these areas. Dust accumulated where no CNTs were embedded-towards the bottom of each gore and on the gore, strips as seen in Figure 18.

While the 50-75 μm showed visibly excellent performance (quantitative numbers in next section), 10-50 μm dust was difficult to drop with uniform coverage over the entire knee. The small grain dust was very cohesive. Therefore, when the dust was dropped over the knee area, it dropped in clusters causing several layers buildup of dust. This impeded the performance and was not immediately comparable to that of 50-75 μm dust clearance. However, one critical observation during the 10-50 μm dust was that, even if clusters of dust adhered to the fabric, when additional dust, was dynamically dropped over these areas already contaminated with dust, the new dust picked up the already adhered dust and visibly cleared the area (bottom picture in Figure 19). For the 10-50 μm , due to challenges with dust loading limited data was usable for the analysis.

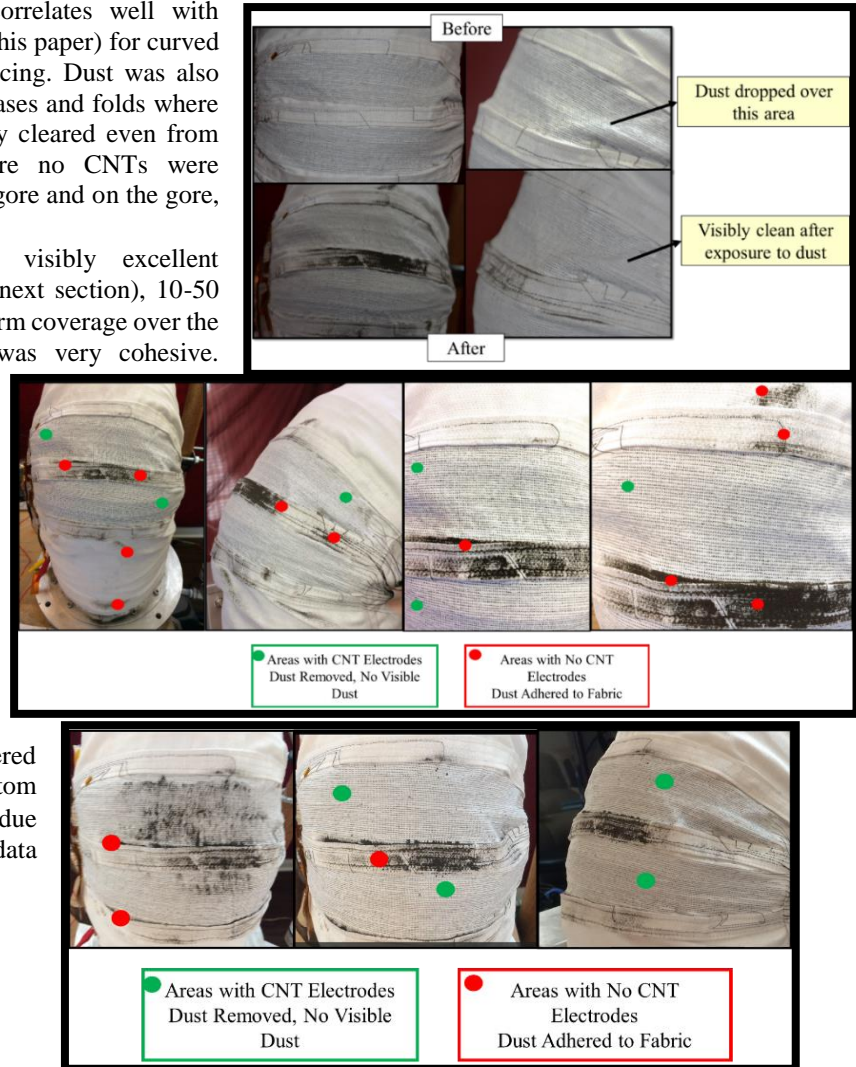


Figure 18[Top] Images of the knee for dynamic dust cleaning operations, [Middle] No visible dust within electrode area; dust collected in areas with no electrodes, [Bottom] Before and after cleaning images of the static dust locating cleaning operations.

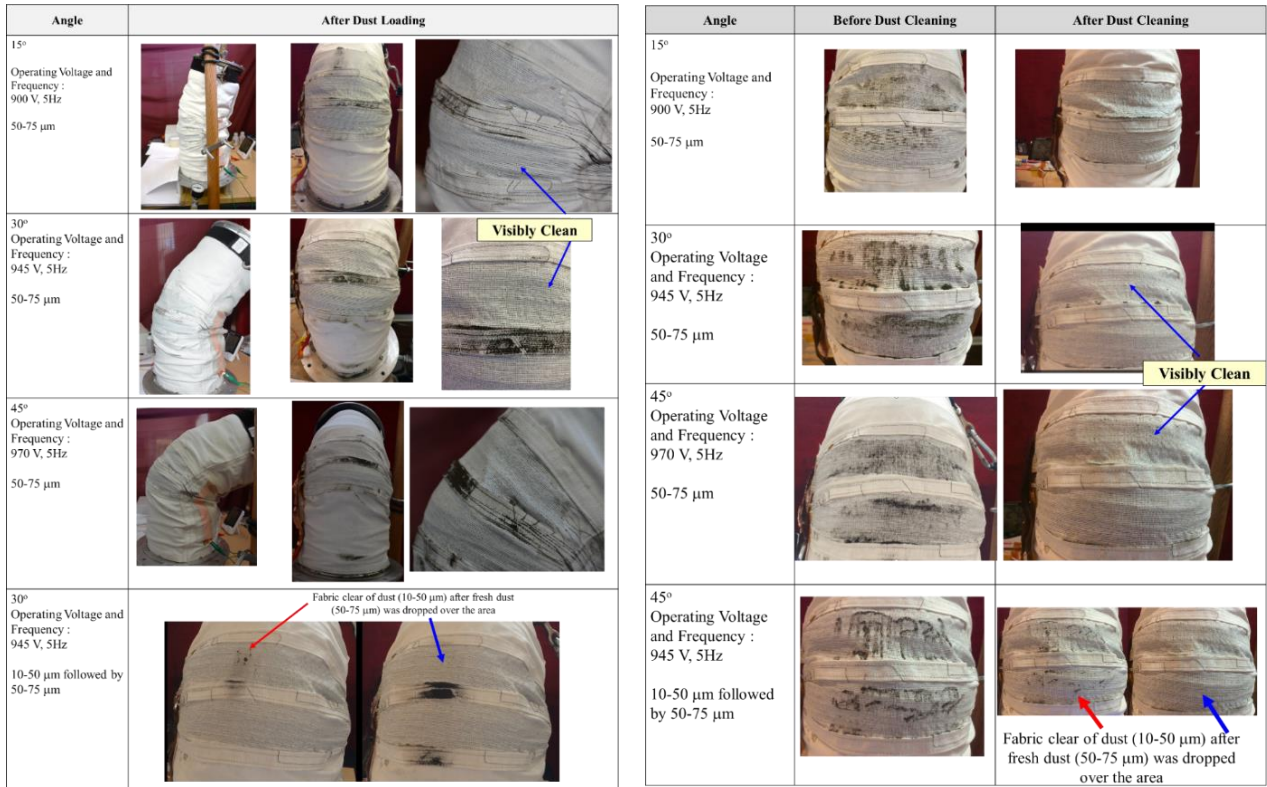


Figure 20. (Left) Dynamic dust condition cleaning results (Right) Static Test results

- Dust Cleaning Performance: Dynamic runs**

Figure 21 illustrates the results on the percentage of area covered by dust after cleaning operations obtained for each knee angle (15°, 30°, 45°) along with results from the coupon test (represented as 0° in the figure). The figure displays the average value of dust coverage calculated over the five sections on two repeated runs for each angle. The parameter used to determine the performance for the dynamic dust setting was the total amount of dust coverage over the knee covered in electrodes after dust cleaning operations derived from ImageJ analysis. For the 50-75 μm dust loading, results show that the system can clear most of the dust dropped over the knee and the percentage of dust covering the knee post cleaning is within 5% of the fabric area at all angles. The difference in performance of the system was minor between all three angles tested, with the 15° position having the highest (5.4%) percentage of area covered by dust. Compared to the coupon tests, the knee experiments show an increase of approximately 2.5% in the dust remaining on the fabric. This minor difference is attributed to the 50-100 V decrease in the operating voltages while performing the knee experiments due to breakdown initiation at a lower voltage due to electrode distance change caused by creases/folds and manufacturing process. The decrease in the operating voltage impacts the electric field produced near the electrodes, thereby

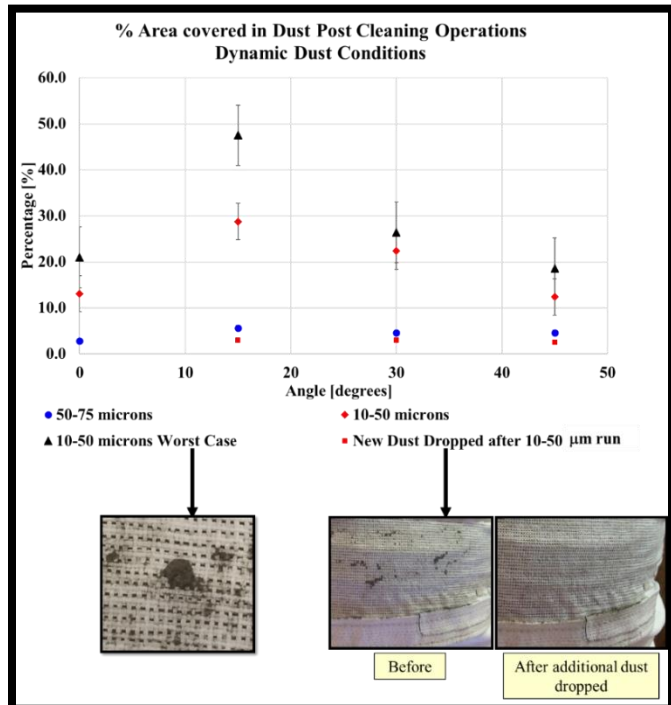


Figure 21. % of fabric area covered in dust after cleaning operations

impacting the performance of dust cleaning ability. In this case the decrease of 100 V for example reduces the electric field produced by 11 % that is translated into the 2.5% increase in the dust covering the fabric. The overall dust coverage however < 10% post cleaning operations for all knee angles. For the 10-50 μm , the biggest challenge was to uniformly distribute the dust during the dynamic dust loading operations. Figure 21 shows that the percentage of the fabric covered in dust after cleaning operations for some runs was >25%. However, the performance of the system for the small grains is inconclusive (includes worst case areas where substantial amounts dropped in a single area (>5g)).

A critical observation made during the experiments was that when 50-75 μm dust was dropped over the residual 10-50 μm dust on the fabric while the system was still active, the new dust removed nearly 95% of the adhered 10-50 μm dust. These values are shown in the lower half of the Figure 21, that show how the % dust coverage from worst case areas represented by (\blacktriangle) reduced to less than 5% dust coverage represented by (\blacksquare). Based on the available data from Apollo missions, the lunar regolith includes ~ 45% of dust between 0-45 μm dust, and roughly 55% of the dust is above grain sizes of 45 μm (See Figure 22). Therefore, the lunar dust is a mixture of assorted sizes and is not isolated to just the 10-50 μm dust as tested in the current experiments. It is anticipated from the available data and observations during the experiments that the mixture of various dust grains would help solve most of the cohesion issues encountered during the 10-50 μm runs and exposure to purely the <50 μm range during lunar operations may be rare. Tests in the future are recommended to be conducted with a mixture of grain sizes ranging from 5-150 μm . This would help evaluate cleaning operations in realistic dust loading conditions on the lunar surface rather than focusing on specific dust sizes due minimizing the cohesive behavior of the dust when isolated to just small grain sizes.

- *Dust Cleaning Performance: Static runs*

Figure 23 illustrates the overall results on the percentage of fabric area covered by dust after cleaning operations for each knee angle (15°, 30°, 45°) along with results from the coupon test (0°). The figure displays the average value of dust coverage over the five sections on two repeated runs for each knee angle. For the 50-75 μm , all five data points for two consecutive runs were utilized. For the 10-50 μm , only limited data points (2-4) points over the two runs per angle were valid since the dust loading on the knee at the various angles was a challenge to uniformly distribute the dust over the knee. Results show that for the 50-75 μm , < 7% of the fabric is covered by dust after cleaning operations. Similar to the dynamic runs, the 10-50 μm dust was very cohesive and did not consistently drop over the fabric. The best-case scenarios showed that after cleaning operations < 20% of the fabric was covered in dust. However, worst case scenarios where clusters of dust dropped and could not be cleared at initial system power on show nearly 30% of the area covered in dust (\blacktriangle). However, when new dust (50-75 μm) was dropped over the adhered dust

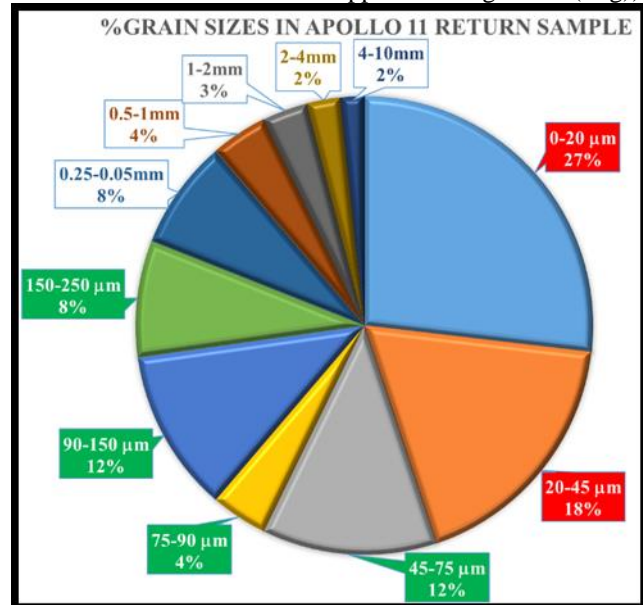


Figure 22. Lunar dust particle size distribution from Apollo 11 sample⁷

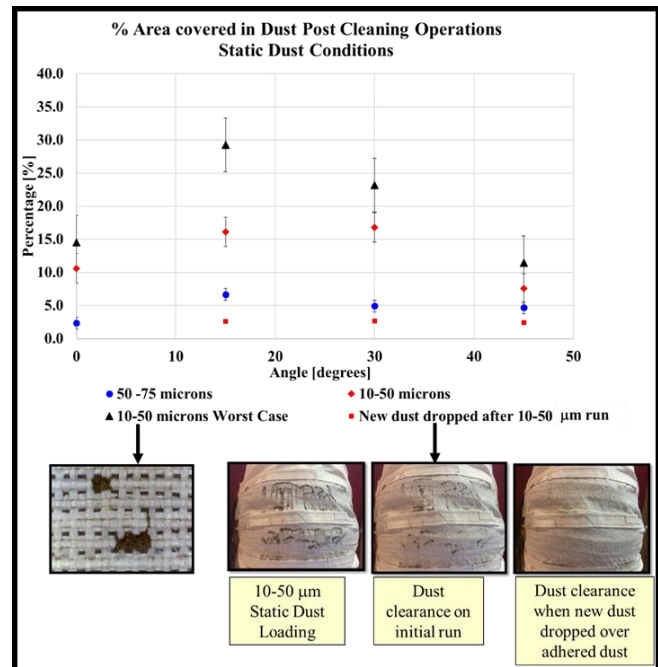


Figure 23. Overall data showing % of fabric covered in dust post dust cleaning operations for the 50-75 μm and 10-50 μm test runs at different angles. The 0° represents data from the coupon tests.

while the electrodes were active, the system could repel the already adhered residual dust bringing the percentage area covered by dust to <5% as shown in the figure (■).

For the 50-75 μm dust, Figure 24 shows the percentage of the fabric covered in dust before and after cleaning operations along with the dust clearing performance (% of dust removed) which is between 92-95%. The system could clear most of the statically adhered dust for all angles of the knee. Comparing the coupon test and the knee results, the percentage dust covering the coupons after dust cleaning was 2.3% compared to the 4.9-7% dust coverage in the current experiments. This difference can be attributed to two things, first the operating voltages for the coupons (0°), 15° and 45° knees angles, were 1000 V, 900-945 V and 970 V respectively. This ~50-100 V decrease in the operating voltage at the 15° angle has a direct impact on the electric field intensity produced (~11% decrease in electric field magnitude from simulation); lower electric field compared to relatively higher electric field value on the coupon tests (0°) because of higher operating voltage. For the 10-50 μm dust loading, even though two consecutive runs were performed, and data was collected, only part of the data was useful due to inconsistencies in being able to load the knee with uniform dust coverage. Figure 25 illustrates the before and after dust coverage and cleaning efficiency. It is noticeable that the efficiency of the system to clear the dust at 15° and 30° is lower (~75%) when compared to the efficiency of the system at 45° and the coupon test (0°). Again, these are attributed to the lower operating voltages at the angles compared to the flat coupon. Additionally, the dust loading condition for the static case using the technique was not efficient as clusters of dust dropped in a small area and could not be distributed evenly. Nevertheless, the overall average amount of dust covering the fabric post cleaning operations is still under 17%.

C. Overall dust cleaning performance

Based on visual observations and ImageJ analysis, the overall performance of the SPIcDER system on the scaled unit shows promising results to further this technology for spacesuit dust cleaning operations. Based on the data, the overall efficiency of the system for a pressurized module at different angles is estimated to be in the range 75-96% depending on particle size and knee angle. The worst-case scenarios are when the knee angle is 15° , specially when tested with the 10-50 μm grain size particles. This reduction is due to lower operating voltages at the angle which was driven by the creases in the fabric, and partly because within these creases there were areas with frayed electrodes that reduced electrode spacing thereby reducing the threshold voltage. However, the performance significantly improved when fresh dust was dropped over the areas where dust already adhered (e.g.: changed from 25% dust coverage to 2% dust coverage). Some of the worst-

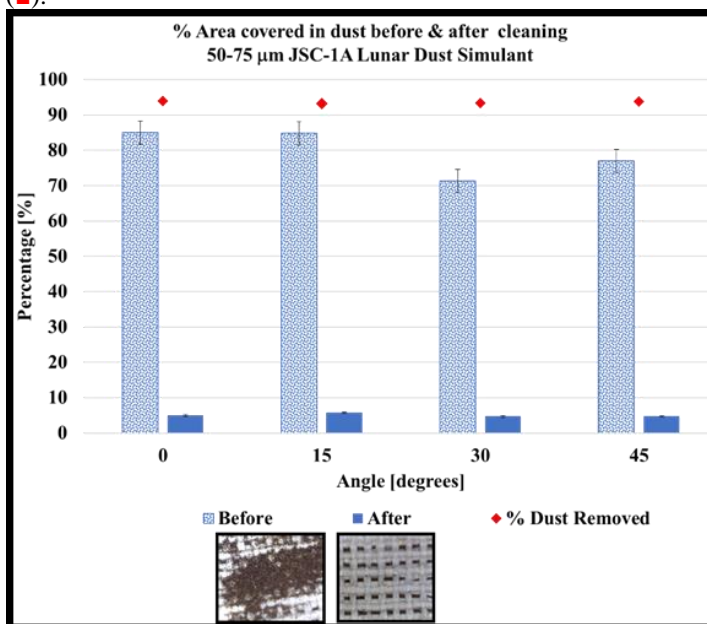


Figure 24. % of area covered in dust before and after cleaning operations for 50-75 μm static dust loading

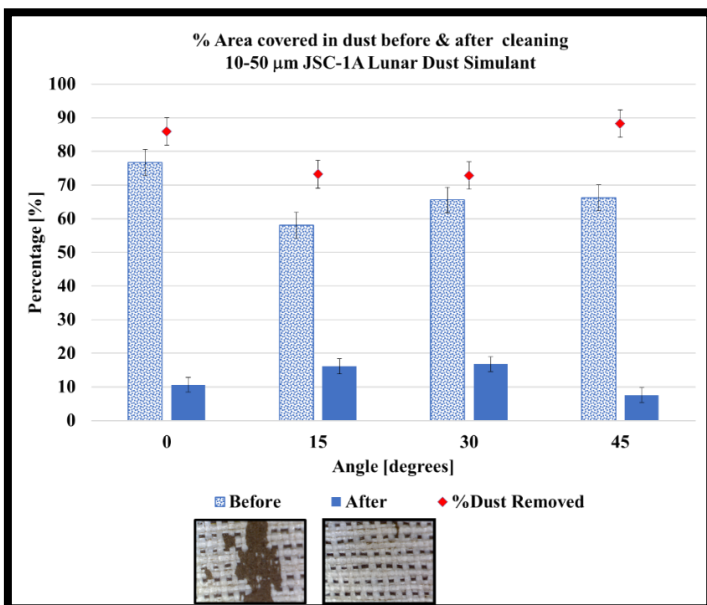


Figure 25. % of area covered in dust before and after cleaning operations for 10-50 μm static dust loading

case scenarios can be prevented using improved manufacturing techniques (described in next section). Table 4. summarizes the performance results from the experiments for the scaled prototype.

Table 4. Summary of dust cleaning performance of the SPICDER system on a scaled unit

Particle Size	% Fabric area covered in dust post cleaning operations		Average % of Dust removed
	Dynamic	Static	$\frac{A_{B_dust} - A_{A_dust}}{A_{B_dust}} \times 100$
50-75 μm	4.4 % [average of all dynamic cases]	5.2% [average of all static cases]	94%
10-50 μm	15.4 % [average of all dynamic cases including worst case with heavy loading]	11 % [average of all dynamic cases including worst case with heavy loading]	87%
Overall Average for 10-75 μm particle size range	10.2 % [Average of all dynamic cases for both particle size range]	8% [Average of all static cases for both particle size range]	90% [average of all runs] [Worst case: 75%, Best case: 96%]
Standard Deviation	5 [All cases for both particle range]	5.1 [All cases for both particle range]	8.3

VI. Recommendations for Improvements in SPICDER Manufacturing and Design

The efficiency of the SPICDER system can be improved by increasing the operating voltages and minimizing electrode overlap by maintaining consistent electrode spacing throughout the length of the parallel electrodes. Recommendations based on lessons learned during building and testing the scaled prototype are detailed here. While some of the suggested recommendations are achievable, they could not be implemented during the duration of this research due to constraints with funding and equipment availability.

A. Manufacturing and Design Improvements

- **Electrode Insulation:** One of the reasons for lower breakdown and operating voltages observed during the experiments was due to fraying of the uninsulated CNT electrode fibers which resulted in and small micron sized fibers sticking out reducing electrode spacing. These can be avoided by insulating the CNT fibers which would align the individual CNT filaments and avoid fraying of fibers, providing an increase in the operating voltages
- **Maintaining consistent electrode spacing:** Automated weaving techniques applied at the fabric making level to prepare the suit fabric would help with inclusion of the CNT fibers early in the manufacturing process. By doing so, the alignment and spacing of the CNT fibers can be precisely controlled. The inconsistencies that were visible during the manual methods can be overcome as the spacing of the warp and weft threads in an automated process can be controlled while manufacturing the underlying fabric as well as by utilizing the required thickness of the warp and weft threads to space the parallel electrodes in a consistent manner. This helps to maintain a consistent breakdown voltage throughout the fabric allowing for consistent operating voltages. If manual methods are utilized, the thickness of the electrodes could be increased to match the thickness of the warp and weft threads to maintain the alignment of the electrodes and consistent spacing between consecutive electrodes. This would also help with increase in the electric field force and the performance is anticipated to improve for smaller grain sizes.

- Avoiding accumulation of dust on the edges: Accumulation of dust on the edges of the gores can be avoided by exploring new electrode arrangement patterns. Two new electrodes arrangements are suggested. 1. Spiral pattern of the electrodes within the gores 2. Longitudinal electrode patterning (orient electrodes perpendicular to the current prototype orientation) (See Figure 26). Also exploring other unique ways of designing the gores to minimize pockets and fabric overlaps would help mitigate this problem.

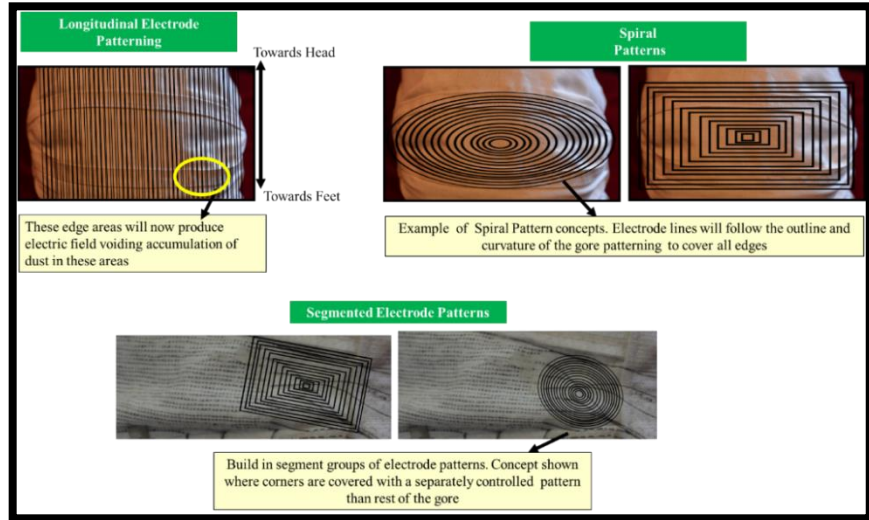


Figure 26. Suggested solutions to improve dust cleaning, avoid areas of accumulation and overcome issues with bunching of fabric.

- Terminal connections: To avoid overlap of the three phase terminals, one set of terminals may be connected on the inside of the fabric. The third set of electrodes can be passed through the backside of the fabric where they can be grouped and terminated to connect to the power system. The specific area on the back side where the electrodes penetrate can be covered with an extra layer of insulating fabric to avoid any contact to the inner layer.

B. Operational Constraints and Improvements

- Pressurized versus unpressurized: The joint-sections of the spacesuit are the most complex sections. The fabric folds and unfolds when the suit is unpressurized and pressurized respectively. The important requirement for stable functioning of the SPIcDER system is to maintain the relative electrode spacing and avoid overlaps. During EVAs, it is ideal to operate the frontal side of the system when the suit is pressurized. Since the posterior side of the suit, especially the knee section will include folds/wrinkles, separate segments of electrode patterns can be implemented on the back side which can be operated post EVAs.
- Variable Voltage Operation: Experiments showed that even with folds at 15° neutral angle, the fabric could repel and remove the dust from these areas. This was accomplished at lower operating voltages (900V versus 1000V) due to the lower threshold voltage. Since the motions of the astronaut during an EVA causes folds, implementing adjustable voltage inputs into the power electronics will aid in changing the input voltage as needed. Input voltage can be adjusted during various positions of the knee while conducting EVA operations, for example when the astronaut is seated on a rover, the knee is fully flexed, allowing an increase in the operating voltage.
- Duty Cycle: It may be beneficial to operate the system in bursts of ~60-120 seconds every 30 minutes during EVA operations when the astronaut comes to a stop/ at set intervals during the EVA. For situations where the astronauts are sitting on a rover with legs in flexed position, they can continuously operate the system. For drilling operations for example, where dust can continuously float and drop over the suit, the SPIcDER system can be activated to minimize dust sticking to the suit.

VII. Conclusion

This research developed a novel concept to address dust contamination of spacesuits for lunar surface operations with extendable application to other flexible surfaces. Leveraging technology built to clean rigid and smooth surfaces, the current research applied CNT fiber technology into the spacesuit outlayer and designed fabrication techniques to create a smart fabric that can autonomously repel dust and protect planetary spacesuits (and similar flexible surfaces) from dust contamination for future planetary exploration missions. Investigations of the SPIcDER system on a scaled joint section of a spacesuit provided insight that the dust cleaning concept proposed in this research is feasible to manufacture and operate over larger sections of a spacesuit (and other similar flexible surfaces). The experiments conducted on the prototype validate the dust cleaning performance observed during small scale demonstrations. From the data analyzed during the scaled tests, the percentage of area covered by dust after implementing the SPIcDER system is in the range 4-16%, below the set requirement of this research of 25%. Furthermore, the dust removing

capability of the SPICDER system is estimated to be between 75-96% on the scaled prototype depending on the dust exposure conditions (dynamic dust versus static dust) for lunar dust simulant with particle sizes between 10-75 μm at three different knee angles. Limitations where lower performance (higher dust coverage of fabric after cleaning and lower dust removal efficiency) was observed is attributed to covering the fabric with several layers of dust, specially the 10-50 μm grain size that was cohesive. However, this was shown to overcome when dust contaminated fabric was exposed to fresh dust. It is anticipated that the lunar dust will include a mixture of 10-150 μm particle sizes. It is estimated that results will improve if future tests utilize appropriate mixture of small and large particle size distributions replicating lunar dust particle size distribution. Recommendations for improving the manufacturability and the cleaning performance of the system have been provided based on lessons learned from the prototype fabrication and experiments.

Acknowledgments

The authors would like to acknowledge Garry Harris of DeLeón Technologies who was key to developing the joint knee section. The authors are also thankful to Dr.Dmitri Tsentalovich at DexMat® for generously providing CNT samples to experiment the new concepts. Special thanks to Richard Rhodes and Amy Ross from NASA Johnson Space Center who generously provided spacesuit material for this research.

References

- ¹ Christoffersen, R., Lindsay, J. R., Noble, S. K., Meador, M. A., Kosmo, J. J., Lawrence, J. A., and McCue, T., "Lunar Dust Effects on Spacesuit Systems: Insights from the Apollo Spacesuits," NASA TP-2009-214786, 2008.
- ² Manyapu, K. K., Peltz, L., de Leon, P., Gaier, J. R., Tsentalovich, D., Calle, C., & Mackey, P., "Investigating the Feasibility of Utilizing Carbon Nanotube Fibers for Spacesuit Dust Mitigation," International Conference on Environmental Systems, Vienna, Austria, 2016
- ³ Manyapu, K.K., "Spacesuit Integrated Carbon Nanotube Dust Mitigation System for Lunar Exploration," Ph.D. Dissertation, Aerospace Science Dept., University of North Dakota, Grandforks, ND, 2017
- ⁴ De Leon, P., and Harris, G., "NDX-2: development of an advanced planetary space suit demonstrator system for the lunar environment," International Conference on Environmental Systems, Portland, OR, 2011
- ⁵ Harris, G. L., *The Origins and Technology of Advanced Extravehicular Space Suits*, AAS History Series, 24, 2001
- ⁶ Gaier, J. R., de León, P. G., Lee, P., McCue, T., Hodgson, E., & Thrasher, J., "Preliminary Testing of a Pressurized Space Suit and Candidate Fabrics Under Simulated Mars Dust Storm and Dust Devil Conditions," NASA/TM-2010-216787. 4International Conference on Environmental Systems, Barcelona, Spain 2010
- ⁷ McKay, David S., and Douglas W. Ming., "Mineralogical and chemical properties of the lunar regolith." *Lunar Base Agriculture: Soils for Plant Growth*, 1989, pp 45-68.